Aerosol Science and Technology

ISSN: 0278-6826 (Print) 1521-7388 (Online) Journal homepage: http://www.tandfonline.com/loi/uast20

Characterization and Response Model of the PPS-M Aerosol Sensor

Antti Rostedt, Anssi Arffman, Kauko Janka, Jaakko Yli-Ojanperä & Jorma Keskinen

To cite this article: Antti Rostedt, Anssi Arffman, Kauko Janka, Jaakko Yli-Ojanperä & Jorma Keskinen (2014) Characterization and Response Model of the PPS-M Aerosol Sensor, Aerosol Science and Technology, 48:10, 1022-1030, DOI: 10.1080/02786826.2014.951023

To link to this article: http://dx.doi.org/10.1080/02786826.2014.951023

Accepted online: 14 Aug 2014.

Aerosol Science and Technology, 48:1022–1030, 2014

ISSN: 0278-6826 print / 1521-7388 online
DOI: 10.1080/02786826.2014.951023

Characterization and Response Model of the PPS-M Aerosol Sensor

Antti Rostedt,[1] Anssi Arffman,[1] Kauko Janka,[2] Jaakko Yli-Ojanperä,[1] and Jorma Keskinen[1]
[1]*Aerosol Physics Laboratory, Department of Physics, Tampere University of Technology, Tampere, Finland*
[2]*Pegasor Oy, Tampere, Finland*

The Pegasor PPS-M sensor is an electrical aerosol sensor based on diffusion charging and current measurement without particle collection. In this study, the role and effect of each component in the instrument is discussed shortly and the results from a thorough calibration measurements are presented. A comprehensive response model for the operation of the PPS-M sensor was developed based on the calibration results and computational fluid dynamics (CFD) modeling results. The obtained response model, covering the effects of the particle charger, the mobility analyzer, and both diffusion and inertial losses, was tested in the laboratory measurements with polydisperse test aerosols, where a good correlation between the model and the measured results was found.

INTRODUCTION

The concern about the health effects of the exposure to fine particles has led to an increasing request for aerosol measurement and monitoring. Aerosol concentration measurement may be realized for various particle properties, such as particle number, mass, surface area, and volume (Kulkarni et al. 2011). Real time aerosol concentration instruments are usually based on the electrical or optical detection techniques. The optical instruments typically utilize light scattering or absorption of particles, while the electrical instruments are most commonly based on charging of the particles and subsequent measurement of the charge carried by the particles as an electrical current.

Particle charging is usually accomplished by unipolar diffusion chargers based on corona discharge, as reviewed, e.g., by Marquard et al. (2006) and Intra and Tippayawong (2009). Because of the simplicity, one of the most straightforward ways to produce an electrical aerosol detector is to combine unipolar diffusion charger with a faraday cup electrometer. The measured quantity is electrical current, which is related to the particle number concentration and particle size. Ntziachristos et al. (2004) demonstrated such instrument for the real time monitoring of active surface area of particles emitted by a diesel engine. Fissan et al. (2007) introduced a similar instrument with a varying charging efficiency for the monitoring of the lung deposited particle surface area. Recent development of these diffusion charger-based instruments has focused on minimizing the size of the instruments to produce handheld instruments. The AeraSense Nanotracker (Marra et al. 2009) and Matter Aerosol DiSCmini (Fierz et al. 2011) are good examples of such instruments, the latter being even able to provide information on the average particle size of the measured aerosol. To make the instrument even smaller, micro-electromechanical (MEMS) techniques have been used by Lee et al. (2011).

All of the electrical instruments mentioned above are based on the collection of the particles after charging. Lehtimäki (1983) demonstrated electrical aerosol instrument without particle collection, based on measuring the charge escaping the charger with the charged particles. The idea has also been applied by Rostedt et al. (2009b). Recently, Fierz et al. (2014) described a non-collecting instrument based on induced current measurement.

The Pegasor PPS-M (Pegasor Oy, Tampere, Finland) sensor treated in this article is based on the escaping charge principle. The basic principle of the sensor has been presented by Lanki et al. (2011). Application of the sensor to engine exhaust measurements has been described by Ntziachristos et al. (2011, 2013). In this article, we present the first detailed calibration of the instrument, and a comprehensive model for the response of the instrument as a function of particle size together with laboratory test measurements.

Received 17 April 2014; accepted 7 July 2014.
Address correspondence to Antti Rostedt, Aerosol Physics Laboratory, Department of Physics, Tampere University of Technology, P.O. Box 692, Tampere FI-33101, Finland. E-mail: antti.rostedt@tut.fi

SENSOR COMPONENTS AND OVERALL RESPONSE

The operation of the PPS-M sensor is based on electrical charging and detection of the charged aerosol particles. The design combines a sheath air-assisted corona charger with an

ejector pump (Tikkanen 2009). A schematic view of the sensor (on the left side) and the actual sensor (on the right side) is shown in Figure 1. The instrument design consists of the following main components: a pre-cut cyclone to prevent the sensor from fouling, an ion source to provide charge to the particles, an ejector pump to provide the sample flow, an ion trap to remove the excess ions and to act as a mobility analyzer for the particles, and an electrometer to measure the charge on the particles.

Charging and Electrical System

The charger and ejector combination is designed so that the flow coming out from the ion production area is mixed with the sample and used as a pump flow in the ejector pump. In the charging region, the particles are charged by diffusion charging. The design of the flow-assisted ion source resembles the design presented already by Whitby (1961). This arrangement has the advantage of keeping the discharge electrode in a clean air flow. The volume of the charging region is rather small, resulting in a relatively low residence time for the charging process.

An ion trap is applied to prevent the charging ions from escaping the instrument and contributing to the charge measurement. In the present design, the trap geometry is annular and the applied electrical field can be varied directly from the user interface. By changing the electrical field, the cut point of the ion trap can be changed. The trap is dimensioned so that it is also able to collect a part of the particles, if the collection voltage is set high enough. This makes the trap to act as a simple zeroth-order mobility analyzer, which gives the possibility to estimate the average particle size of the measured aerosol. For this, the shape of the size distribution must be either known or assumed. This technique has earlier been used for particle density measurement by Rostedt et al. (2009a).

The electrical current measurement is realized without collecting the particles, by measuring the net current leaving the instrument. As a consequence, the response of the instrument depends on the initial charge state of the input aerosol and any ion leakage out from the instrument. Because of this escaping current measurement technique, the power sources for the corona charger and ion trap are isolated from the ground. Since the current is measured with a high sensitivity electrometer between the isolated virtual ground and the ground potential, both a low noise level and a high isolation resistance are required for the isolation. The electrometer is realized using an operational amplifier with a capacitive feedback circuit. Because of the electrometer design, the voltage difference between the two measurement points is well below 1 mV (Keithley Instruments Inc. 2004). For the practical use of the sensor, the sampling rate of the electrometer and the low pass filtering of the measured signal can be altered to suit the application in question.

Flow System

Computational fluid dynamics (CFD) simulation was used for optimizing the flow system of the sensor design. It was primarily used during the design process to estimate the ejector performance and the turbulent flow patterns inside the sensor. The CFD simulations also provided information on the diffusion losses within the whole sensor. The flow fields inside the sensor were modeled using Ansys Fluent 14.0. For the three-dimensional simulations, SST-k-ω turbulence transfer model was employed, and the computation grid consisted of 2.3 million cells. Boundary conditions at the flow boundaries were pressure inlets and pressure outlets.

The design of the ejector pump was optimized for minimizing the pressurized air consumption, while still providing enough pressure difference to provide an adequate sample

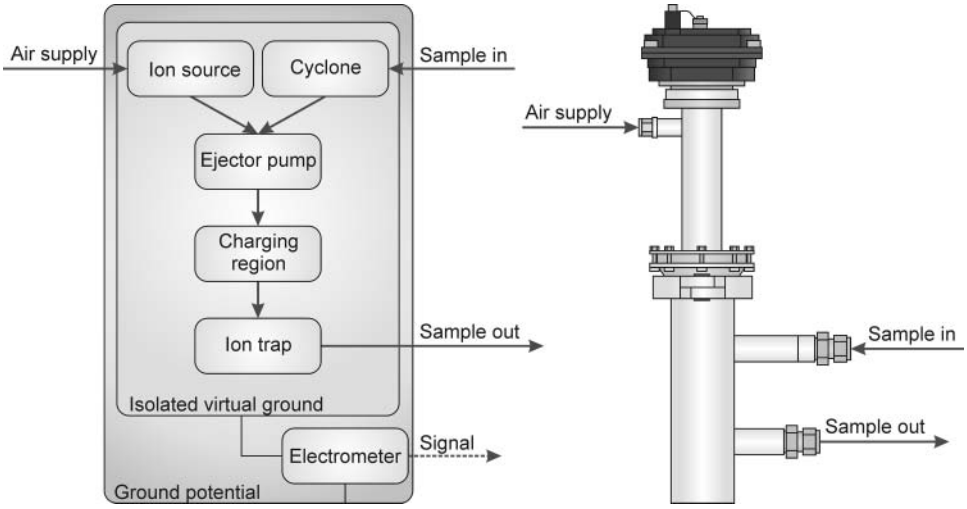

FIG. 1. Schematic view of the sensor components on the left and picture of the sensor on the right.

flow in a practical measurement setup. The needed pressure difference was minimized by returning the ejector outlet to the same pressure with the sample. Practically, this means that in the sensor there is two connections for the sample flow; one delivering the sample into the sensor and the other returning the sample, pump flow, and needed sheath air flows to the same pressure where the sample is taken.

The CFD modeling indicated the flow to be turbulent in the mobility analyzer region. The turbulence leads to less steep collection efficiency curves, which limits the size resolution of the analyzer. However, this is considered acceptable since the information from the mobility analyzer is only used for estimating the median size for the measured size distribution.

Sensor Response

All the sensor components contribute to the sensor response and from a calibration point of view the combined overall response would be enough. However, in the current design the operation of the sensor can be altered by the user by varying the mobility analyzer collection voltage. For this reason, more thorough understanding on the response is required. The charger charging efficiency E_{ch} and the mobility analyzer penetration P_{ma} are the main contributors to the overall response, while the effect of the non-electrical components, such as inertial and diffusion losses, plays a smaller role. The combined sensor response R is a function of the particle size d_p and the mobility analyzer voltage V_{ma}. It has the form of Equation (1), where the diffusion and inertial losses are expressed as penetrations P_d and P_i, respectively:

$$R(d_p, V_{ma}) = E_{ch}(d_p, V_{ma}) P_{ma}(d_p, V_{ma}) P_d(d_p) P_i(d_p) \quad [1]$$

Because of the complicated flow path and the integrated nature of the sensor design, it was not possible to measure the effect of each component individually. The term P_d describing the diffusion losses was obtained from the CFD simulations, while the effects of the remaining components were calculated from the calibration results.

EXPERIMENTAL

The objective of the calibration measurements was to find out the sensor response to particle number concentration as a function of the particle mobility size together with the particle collection characteristics of the mobility analyzer. The calibration measurements were started by first verifying the operation of the integrated electrometer. For this, a reference electric current source, providing currents from 100 fA to 40 pA, was used. To ensure the correct current levels, the source was first calibrated using a Keithley 6430 Remote SourceMeter (Keithley Instruments Inc., Cleveland, OH, USA).

Sensor Response

In the response calibration, the Single Charged Aerosol Reference (SCAR; Yli-Ojanperä et al. 2010) was used as an aerosol generator. The main advantage of the SCAR is that it produces a nearly monodisperse aerosol sample with particles containing only one elemental charge each. The generated aerosol was then classified by a differential mobility analyzer (DMA model 3071A, TSI Inc., Shoreview, MN, USA). As a result a truly monodispersed aerosol was obtained for the calibration measurements. The DMA was used with recirculating sheath air flow with the flow rate range of 3 to 10 lpm, while the sample flow was varied from 1 to 2 lpm. With these flow rate values, the particle size range for the monodisperse calibration aerosol was 20–920 nm. Although the used sheath air to sample flow rate ratios were not optimal for the best size resolution of the DMA, the flow rates were chosen in order to cover a wide particle size range and to maximize the particle output after the classification. The flow rate of the recirculated DMA sheath flow was monitored and controlled by a custom made flow controller unit calibrated with an air flow calibrator (Gillian

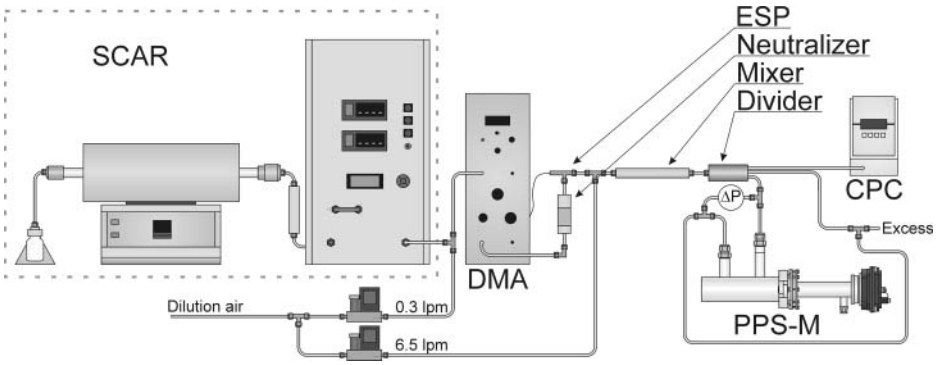

FIG. 2. The measurement setup used in the calibration. The SCAR was used as an aerosol source, the DMA for size classification and the CPC acted as the reference instrument.

Gilibrator-2, Sensidyne, LP, St. Petersburg, FL, USA). The whole measurement setup is shown in Figure 2.

In order to minimize the effect of the initial charge of the particles to the sensor response, the aerosol was neutralized using an ^{85}Kr aerosol neutralizer (Model 3077, TSI Inc., Shoreview, MN, USA). To ensure proper operation of the neutralizer, a small feed of pressurized air, 0.3 lpm, was introduced to the sample flow before the neutralizer. This was needed since the SCAR device produces the particles in a nitrogen atmosphere. After the neutralizer, the excess ions were removed by a small electrostatic precipitator (ESP). Because the total volumetric flow rate needed for the instruments was higher than the output of the classifying DMA, the sample was diluted by a second flow of pressurized air. Both dilution air flows were controlled with mass flow controllers (Alicat Scientific Inc., Tucson, AZ, USA) and the second dilution air flow was set to a level, which ensured a small excess flow from the sample line. After the dilution, a static mixer (Kenics 37-06-110, Chemineer, Dayton, OH, USA) was added to ensure proper mixing of the produced aerosol and dilution air. The sample was then divided with a flow divider (Model 3708, TSI Inc., Shoreview, MN, USA) into three parts: one for the sensor, one for a reference Condensation Particle Counter (CPC Model 3772, TSI Inc., Shoreview, MN, USA), and one for an excess flow. In order to ensure good accuracy in the number concentration measurement, the detection efficiency of the CPC used as a reference was calibrated with the method described in Yli-Ojanperä et al. (2012).

During the measurements, the pressure difference between the sensor inlet and outlet flows was monitored to ensure the correct sample flow into the sensor. During the measurements, the differential pressure was 165 Pa, sensor inlet being in a slightly lower pressure. This underpressure is low compared to the maximum pressure difference of 4.7 kPa, which the sensors ejector pump can supply with zero sample flow. The volumetric sample flow rate measured at the calibration conditions, i.e., with the same pressure difference, was 6.40 lpm and for the ejector pump flow a value of 3.63 lpm was measured after the calibration. For the measurements, the electronics was set up for 1 Hz sample rate with 3 s digital first-order low pass filter. With these settings, the short-term noise level of the measuring electronics was around ± 1 fA. The instrument and sample gas temperature was 296 ± 3 K.

Mobility Analyzer

The measurement setup also provided the possibility to calibrate the mobility analyzer of the sensor with the help of the singly charged particles. For the mobility analyzer calibration, the measurement setup was almost the same described above, only the aerosol neutralizer and the ESP were removed from the setup. Additionally, the charger inside the sensor was turned off. In this measurement, the singly charged particles were collected by the mobility analyzer inside the sensor, resulting in a current measured by the sensor electrometer. The polarity of the current was inverted compared to the normal operation, since instead of escaping out from the sensor the particles were collected inside the sensor. The desired quantity from the measurement was the fraction of particles collected by the mobility analyzer. The measured quantities were the current caused by the collected particles and the number concentration at the sensor inlet. This means that the current measured by the sensor needed to be converted to a particle number. For this, the charge state of the particles must be known. By using the SCAR as an aerosol source, all the particles are known to have a single elementary charge with the uncertainty of 0.16% (Högström et al. 2011).

RESULTS

To find out a model for the sensor response, the effect of each sensor component needs to be studied individually. For the diffusion losses, the results from the CFD simulations were used. For the effects of the other components, the parameters of the model were fitted to the calibration results. The flow system performance was also verified by measuring the sample flow rate and the maximum pressure the ejector can produce. These values were compared to the values obtained by CFD simulation. SI units were used for the parameters of the model, except for the charging efficiency and the overall response. Those are expressed in units of fAcm^3 for convenience.

Flow System Performance and Diffusion Losses

The nominal sample inlet flow was measured with minimal pressure difference between the sample inlet and outlet. To find out the maximum underpressure for the ejector with zero sample flow, a differential pressure meter was connected to the sample inlet. For the measurement, a nominal supply air pressure of 0.15 MPa was used. The measured result together with the corresponding results from the CFD simulations are collected to Table 1. Although there are some differences, the agreement between the measured values and the simulation results is good.

Diffusion losses inside the sensor were simulated in Eulerian fashion. Aerosol was fed to the sensor as a component of

TABLE 1
Parameters of the ejector flow system. CFD simulation results compared to the measured values

Parameter	CFD	Measured
Pump flow pressure (MPa)	0.15	0.15
Pump flow rate (lpm)	3.2	3.63
Ejector maximum underpressure (kPa)	4.3	4.7
Nominal sample flow rate (lpm)	6.9	6.70
Cyclone cut point (μm)	$\sim$2.0	—

the gas mixture. The boundary condition for aerosol concentration at the wall boundaries was zero in order to calculate the diffusion flux of particles to the sensor walls. Laminar diffusion coefficient was then adjusted to match the different size particles (Stokes–Einstein relation was used for the diffusion coefficient; Hinds 1999). Turbulence enhances the diffusion inside the sensor, and this was taken into account by using the effective diffusion coefficient for the aerosol mixture component. The effective diffusion coefficient is a sum of the laminar and turbulent diffusion coefficients, where the turbulent coefficient is computed from the turbulent transfer model (SST-k-ω) according to the Fluent standard formulation (ANSYS 2011). The computation grid was tetrahedral, and adapted several times until the results were unaffected by further improvements. The dimensionless wall coordinate y+ was in the range 0.1–3 in the final grid. Next, a functional form of diffusion losses was fitted to the CFD results. Despite the fact that the flow inside the sensor is mostly turbulent, it was found that the transport efficiency for laminar flow through a cylindrical tube gives the best fit for the modeled diffusion losses. According to Gormely and Kennedy (1949), the transport efficiency has the form of Equation (2), which is a function of the particle (laminar) diffusion coefficient D_p multiplied by a fitted parameter $\mu_0 = 1.79 \times 10^5$ s/m^2. The parameter μ_0 value corresponds to diffusion losses of a 6 m long tube in laminar flow conditions with the sample inlet flow rate. The unit for the diffusion coefficient is m^2/s.

$$P_d(D_p) = \begin{cases} 1 - 2.56(\mu_0 D_p)^{2/3} + 1.2\mu_0 D_p + 0.177(\mu_0 D_p)^{4/3} \\ \quad \mu_0 D_p < 0.03 \\ 0.819e^{-3.657\mu_0 D_p} + 0.097e^{-22.3\mu_0 D_p} + 0.032e^{-57\mu_0 D_p} \\ \quad \mu_0 D_p \geq 0.03 \end{cases} \quad [2]$$

Mobility Analyzer

The collection of charged particles in the cylindrical mobility analyzer in the case of turbulent plug flow is obtained using the equation derived by Deutsch in the 1920s. The penetration efficiency of the particles can consequently be written as

$$P_{\mathrm{ma}}(d_p, V_{\mathrm{ma}}) = e^{-\frac{neC_c}{3\pi\eta_g d_p Z_0(V_{\mathrm{ma}})}} \quad [3]$$

The term in the exponent is the collection efficiency of the same geometry in laminar flow conditions, which can be expressed as the ratio of the particle electrical mobility to the limiting electrical mobility Z_0. The electrical mobility is a function of the particle size d_p. The other terms needed are the number of charges per particle n, the elementary charge e, the slip correction factor C_c, and the gas viscosity η_g. The limiting electrical mobility is the minimum electrical mobility that would cause 100% collection efficiency for laminar flow conditions. It is a value specific to the geometry and can be obtained from the dimensions of the analyzer with the help of the Equation (4). The dimensions needed are the inner and outer diameters, $s_i = 0.022$ m and $s_o = 0.030$ m, length $l_e = 0.032$ m of the analyzer, the volumetric flow rate inside the analyzer Q_{tot}, and the applied voltage V_{ma}. The flow rate Q_{tot} is a sum of the volumetric flow rates of the sample flow Q_s and the ejector pump flow Q_p in the conditions of the mobility analyzer. As seen from Equation (4), the limiting electrical mobility in the laminar flow conditions is directly proportional to the total flow rate and inversely proportional to the applied voltage. All the remaining terms can be combined to a single constant K:

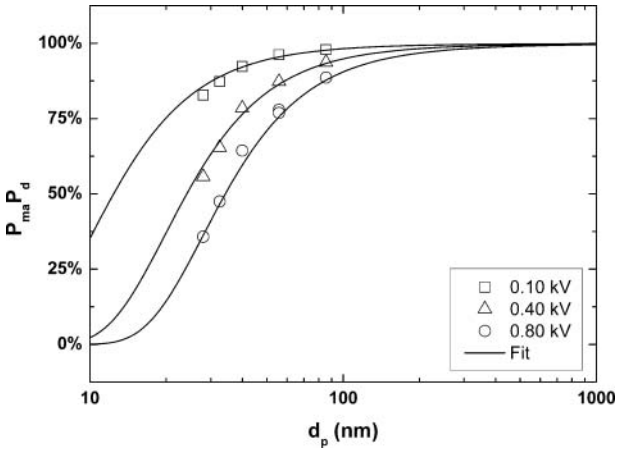

FIG. 3. Ion trap acting as a mobility analyzer: particle penetration efficiencies with different trap voltages. Open symbols are the penetration efficiencies measured with singly charged particles and the solid line is the penetration according to the fitted model.

$$Z_0(V_{\mathrm{ma}}) = \frac{Q_{tot}\ln\left(\frac{s_o}{s_i}\right)}{2\pi V_{\mathrm{ma}} l_e} \Rightarrow Z_0 = \frac{(Q_s + Q_p)K}{V_{\mathrm{ma}}} \quad [4]$$

The diffusion losses also contribute to the mobility analyzer penetration efficiency and the effect was taken into account. The fit for the $P_{\mathrm{ma}}P_d$ product, drawn in Figure 3, is obtained using Equations (2)–(4) with the value $K = 1.37$ m^{-1} for the constant. This value gives the best fit to the measured data, although it differs slightly from the value calculated from the mechanical dimensions $K_{\mathrm{teor}} = 1.54$ m^{-1}. As seen in Figure 3, the penetration efficiency is over 90% for particles larger than 100 nm with all mobility analyzer collection voltages.

Charging Efficiency and Average Number of Charges

The sensor response was obtained from the ratio of the current measured with the sensor to the number concentration measured by the CPC. The response decreases as the mobility analyzer voltage is increased, since increasing part of the small

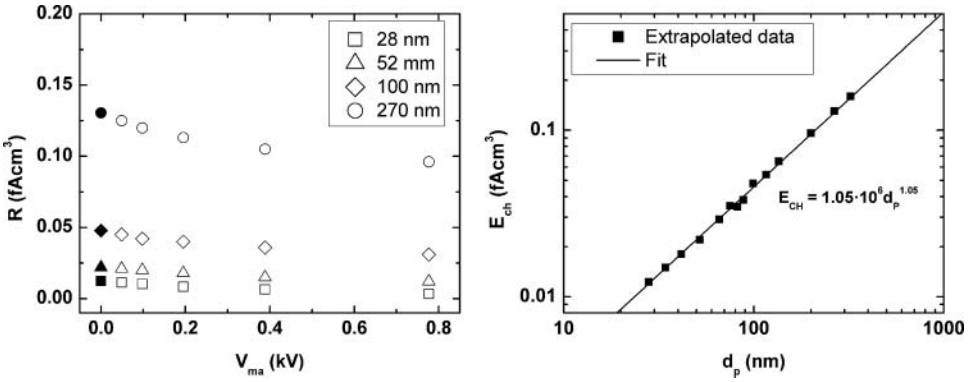

FIG. 4. Left: measured sensor responses (open symbols) as a function of the applied trap voltage together with the extrapolated responses (closed symbols). Right: the extrapolated sensor response points with zero trap voltage (closed symbols) with the power function fit (line) as a function of the particle size.

particles is collected by the mobility analyzer. For the sensor response, a model for the charging efficiency of the charger E_{ch} is needed. Typically, in unipolar diffusion chargers, the charging efficiency is approximated by a power function described by Equation (5), where the parameters a and b are obtained by fitting to calibration measurements (Kulkarni et al. 2011).

$$E_{\mathrm{ch}}(d_p) = a d_p^b \qquad [5]$$

Because of the ion leakage, it is not possible to have a calibration measurement for the charging efficiency without the effect of the mobility analyzer. This issue was solved by plotting the sensor responses measured for different mobility analyzer voltages as a function of the applied voltage for different particle sizes. Then the responses were extrapolated with a cubic Hermite spline to zero voltage, resulting in an estimate for the maximum charging efficiency without the effect of the mobility analyzer. The plot on the left-hand side of Figure 4 shows an example of the extrapolation. In the plot, the open markers show the measured sensor responses as a function of the mobility analyzer voltage for selected particle sizes and the closed markers show the extrapolated values for zero trap voltage. The extrapolated values for different particle sizes are collected to the plot on the right-hand side of Figure 4 as a function of the particle size. For the extrapolation, only calibration results from particle sizes below 350 nm were used in order to exclude the effect of the inertial losses. From the extrapolated data, the values for the parameters a and b in Equation (5) were obtained.

The main component in the charger efficiency is the product of the particle penetration through the charger and the average number of elementary charges the particles acquire during charging. Usually the value of the product is enough for the use of the diffusion charger (Marjamäki et al. 2000), but in this case the average number of charges per particle is separately needed in order to calculate the collection efficiency of the mobility analyzer. The number of charges could in principle be obtained by measuring separately the particle charge (via electrical mobility) after the charger or the particle penetration (of charged particles) through the charger. Since thorough measurement of either would be laborious, the following approximation is used instead. The results in Figure 3 presenting the penetration efficiencies measured with charger *off* for singly charged particles at different trap voltage settings indicate that a constant value of 100% could be used as a first approximation for the penetration with charger *off*. This is because the experimental penetration efficiencies are nearly 100% at large particle sizes. To check that the approximation applies also for the charger *on* case, the penetration was experimentally determined using 100 nm monodisperse particles for the charger *on* and charger *off* case. The penetration through the charger for *on* and *off* cases was found to be equal and high, over 95%. Based on this, it was assumed that the particle losses inside the charger are negligible, excluding the separately calculated effects of the electrical collection within the trap, the diffusion losses, and the inertial losses. The average number of elementary charges per particle was then estimated to be equal to the charging efficiency divided by the flow rate and the elementary charge. This somewhat underestimates the number of elementary charges of the charged particles, but is expected to be reasonable when limited to a minimum value of one. The resulting functional form is shown in Equation (6), where particle diameter is in meters:

$$n_{\mathrm{AVE}}(d_p) = \begin{cases} 1, & d_p < 1.63 \cdot 10^{-8}\,\mathrm{m} \\ 6.13 \cdot 10^7 d_p^{1.05}, & d_p \geq 1.63 \cdot 10^{-8}\,\mathrm{m} \end{cases} \qquad [6]$$

It turned out that the mobility analyzer collection voltage affects the sensor response more than can be explained by the mobility analyzer collection efficiency. The fact that the difference was seen throughout the measured size range suggests

that the applied collection voltage affects slightly the particle charging efficiency. It is possible that the ion losses in the charging region increase with increasing collection voltage. In order to take the effect into account, a functional form for the parameter a was fitted. In the fitting process, calibration results from particle sizes 200–400 nm were used in order to minimize the effect of the mobility analyzer and the inertial losses. The resulting final form for charger efficiency, Equation (7), was obtained. The unit for the charging efficiency is fAcm^3, the unit for the voltage is V, and the unit for the particle diameter is m:

$$E_{\mathrm{ch}}(d_p, V_{\mathrm{ma}}) = \left(1.05\cdot 10^6 - 7.23\cdot 10^4 \ln\left(1 + 1.12\cdot 10^{-2} V_{\mathrm{ma}}\right)\right) d_p^{1.05} \quad [7]$$

Inertial Losses

As a final step for the sensor response, a fit for the inertial losses in the flow system is needed. For simplicity, it is assumed that for particles larger than 400 nm, the difference between the measured response values and the values obtained using Equation (7) is caused by inertial losses. A simple equation was fitted to the results as

$$P_i(d_a) = 1 - \frac{1}{1 + \left(\frac{6.36\cdot 10^{-7} m}{d_a}\right)^{2.06}} \quad [8]$$

This form has been used to describe inertial impactors (Dzubay and Hasan 1990). Since the particle density affects the inertial losses, the term d_a in the equation is the aerodynamic particle diameter. The fitted parameters are the cut point (636 nm) and the slope of the penetration curve (2.06). Based on the fact that the flow field inside the sensor is turbulent, it is possible that there are turbulence-induced impaction losses inside the sensor. This would explain the rather low response for the large particles.

Sensor Response

The overall sensor response is a particle size-dependent function formed as the product of the charging efficiency E_{ch}, the ion trap penetration P_{ma}, and the particle penetration after inertial and diffusion losses, described by the two penetration terms P_i and P_d as shown in Equation (1). The overall response describes the relation between the inlet number concentration and the sensor output as a function of the particle size. The sensor response with different trap voltages is plotted in Figure 5, where also the measured calibration points and the maximum charging efficiency of the charger are plotted as reference. The inertial losses in the plotted response are calculated with a density value of 912 kg/m^3, which is the density of the particles used in the calibration measurements.

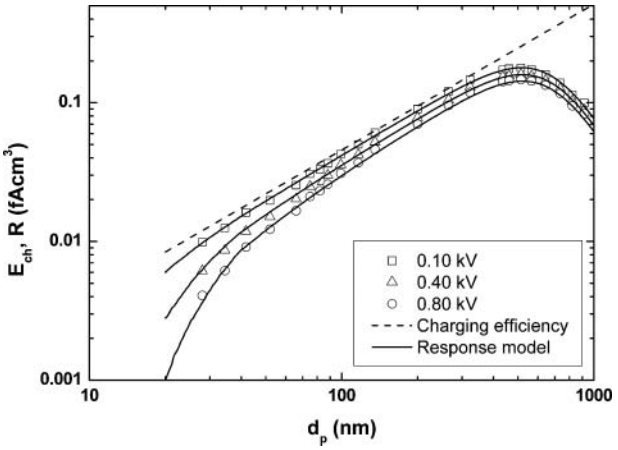

FIG. 5. Measured calibration points (open symbols) together with the fitted PPS-M sensor response as a function of the particle size with different trap voltages (solid line). The dashed line represents the maximum charging efficiency (E_{ch}) of the charger. For the inertial losses a density value of 912 kg/m^3 is used.

Tests with Polydisperse Aerosol

After the calibration, the sensor model was tested in laboratory conditions with polydisperse test aerosol. The measured sensor signals were compared to the simulated signals calculated from the measured size distributions according to Equation (9). The simulated sensor output is obtained by integrating the product of the sensor response $R(d_p,V_{\mathrm{ma}})$ of Equation (1) and the particle number concentration $N(d_p)$ over the particle size. The different components of the sensor response are given by Equations (2), (3), (7), and (8).

$$\begin{aligned} I_{\mathrm{simulated}} &= \int R(d_p, V_{\mathrm{ma}}) N(d_p) dd_p \\ &= \int E_{\mathrm{ch}}(d_p, V_{\mathrm{ma}}) P_{\mathrm{ma}}(d_p, V_{\mathrm{ma}}) P_d(d_p) \\ &\quad \times P_i(d_p) N(d_p) dd_p \end{aligned} \quad [9]$$

During the tests, the median size of the test aerosol was varied between 35 and 120 nm, while the geometric standard deviation (GSD) of the distribution varied from 1.4 to 1.5. Different mobility analyzer collection voltages were also used in the range of 100–800 V. A scanning mobility particle sizer (SMPS, TSI Inc., Shoreview, MN, USA) was used as the reference instrument. In the measurement setup, the pressure difference between the sensor inlet and outlet was monitored in order to avoid too high pressure difference and the actual sensor inlet flow rate was measured and compensated in the simulations. Additionally, good care was taken in order to ensure equal particle concentrations for both instruments. A correlation plot of the measured and the simulated sensor signals is shown in Figure 6. As seen from the figure, the measured signals correlate very well with the simulated signals, although the measured signal is systematically 13% higher. The

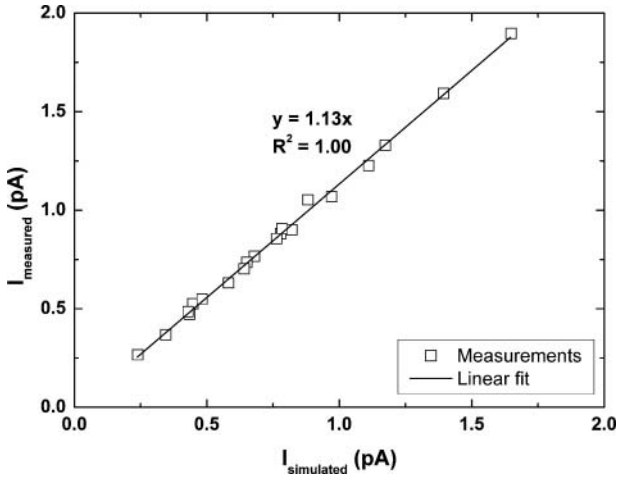

FIG. 6. Correlation plot of the measured and simulated sensor signals in the polydisperse test aerosol measurements.

difference between the measured and simulated values is most likely caused by the combined effect of the detection efficiency of the SMPS and the decreased concentration measurement accuracy caused by flow unbalance within the SMPS DMA. Instead of the sheath air recirculation used in the calibration measurements, the DMA flow rates were measured separately with the integrated mass flow meters that are calibrated on an annual basis. While this ensures good accuracy for the DMA total flow rate and consequently good accuracy on the particle size measurement, it does not ensure a good balance of the sample and monodisperse flows. This possible unbalance leads to a decreased accuracy for the particle concentration measurement.

CONCLUSIONS

In this article, calibration results together with a comprehensive model for the response of the PPS-M sensor were presented. The sensor was calibrated with monodisperse test aerosol, produced with the single charged aerosol reference (SCAR) by using calibrated condensation particle counter (CPC) as the reference instrument. The used calibration setup provided the possibility to have a calibration also for the sensors integrated mobility analyzer. CFD modeling results, used primarily to aid the sensor design, were used as a starting point for the sensor response model. The model covers the effects of the charging efficiency of the charger together with the average number of elementary charges it produces to the particles, the collection efficiency of the mobility analyzer, and both diffusion and inertial losses for the particles. The obtained model fits very well to the calibration data. Although the mobility analyzer is not ideal for mobility classification, the mobility analyzer part of the model is in good agreement with both the measured collection efficiencies and the expected collection efficiency based on the mechanical dimensions. The overall response model was also tested in the laboratory measurements with polydisperse test aerosols and the results were in good agreement with the model.

In applications, where the particle size distribution stays relatively stable and a good approximation can be made for the distribution, it is possible to calculate conversion factors with the help of the model. These factors can be used in converting the sensor output to number, surface area, or mass concentration. The accuracy of the conversion depends on the accuracy of the size distribution approximation. The model brings also more insight on the instrument performance for the data analysis.

FUNDING

This work was conducted within the Measurement, Monitoring and Environmental Assessment (MMEA) research program of CLEEN Ltd., supported by Tekes.

REFERENCES

ANSYS Inc. (2011). *ANSYS Fluent Theory Guide*, 14th release. ANSYS Inc., Canonsburg, PA.

Dzubay, T. G., and Hasan, H. (1990). Fitting Multimodal Lognormal Size Distributions to Cascade Impactor Data. *Aerosol Sci. Technol.*, 13(2): 144–150.

Fierz, M., Houle, C., Steigmeier, P., and Burtscher, H. (2011). Design, Calibration, and Field Performance of a Miniature Diffusion Size Classifier. *Aerosol Sci. Technol.*, 45(1):1–10.

Fierz, M., Meier, D., Steigmeier, P., and Burtscher, H. (2014). Aerosol Measurement by Induced Currents. *Aerosol Sci. Technol.*, 48:350–357.

Fissan, H., Neumann, S., Trampe, A., Pui, D., and Shin, W. (2007). Rationale and Principle of an Instrument Measuring Lung Deposited Nanoparticle Surface Area. *J. Nanopart. Res.,* 9:53–59.

Gormely, P. G., and Kennedy, M. (1949). Diffusion from a Steam Flowing through a Cylindrical Tube. *Proc. R. Irish Acad.,* 52:163–169.

Hinds, W. C. (1999). *Aerosol Technology. Properties, Behaviour and Measurement of Airborne Particles*. Wiley, New York.

Högström, R., Yli-Ojanperä, J., Rostedt, A., Iisakka, I., Mäkelä, J. M., Heinonen, M., et al. (2011). Validating the Single Charged Aerosol Reference (SCAR) as a Traceable Particle Number Concentration Standard for 10 nm to 500 nm Aerosol Particles. *Metrologia*, 48:426–435.

Intra, P., and Tippayawong, N. (2009). Progress in Unipolar Corona Discharger Designs for Airborne Particle Charging: A Literature Review. *J. Electrostat.,* 67(4):605–615.

Keithley Instruments Inc. (2004). *Low Level Measurement Handbook*, 6th ed., Keithley Instruments Inc., Cleveland, OH.

Kulkarni, P., Baron, P. A., and Willeke, K. (2011). Introduction to Aerosol Characterization, in *Aerosol Measurement: Principles, Techniques, and Applications*, P. A. Baron, P. Kulkarni, and K. Willeke, eds., John Wiley & Sons, Hoboken, NJ, pp. 3–13.

Lanki, T., Tikkanen, J., Janka, K., Taimisto, P., and Lehtimäki, M. (2011). An electrical sensor for long-term monitoring of ultrafine particles in workplaces. *J. Phys.: Conf. Ser.,* 304:012013. Available at http://iopscience.iop.org/1742-6596/304/1/012013

Lee, S. G., Hyun, J., Park, D., Hwang, J., and Kim, Y. J. (2011). Application and Performance Test of a Micro-Machined Unipolar Charger for Real-Time Measurements of Exhaust Particles from a Diesel Engine Vehicle. *J. Aerosol Sci.,* 42:747–758.

Lehtimäki, M. (1983). In Modified Electrical Aerosol Detector. in *Aerosols in the Mining and Industrial Work Environments*, Vol. 3, V. A. Marple, and B. Y. H. Liu, eds., Ann Arbor Science Publishers, Ann Arbor, pp. 1135–1143.

Marjamäki, M., Keskinen, J., Chen, -R., and Pui, D. Y. H. (2000). Performance Evaluation of Electrical Low Pressure Impactor (ELPI). *J. Aerosol Sci.*, 31:249–261.

Marquard, A., Meyer, J., and Kasper, G. (2006). Characterization of Unipolar Electrical Aerosol Chargers-Part II: Application of Comparison Criteria to Various Types of Nanoaerosol Charging Devices. *J. Aerosol Sci.*, 37 (9):1069–1080.

Marra, J., Den Brink, W., Goossens, H., and Kessels, S. (2009). Nanoparticle Monitoring for Exposure Assessment Nanotechnology Magazine. *IEEE* 3:6–13.

Ntziachristos, L., Amanatidis, S., Samaras, Z., Janka, K., and Tikkanen, J. (2013). Application of the Pegasor Particle Sensor for the Measurement of Mass and Particle Number Emissions. *SAE Int. J. Fuels Lubr.,* 6(2): 521–531.

Ntziachristos, L., Fragkiadoulakis, P., Samaras, Z, Janka, K., and Tikkanen, J. (2011). Exhaust Particle Sensor for OBD Application. *SAE Technical Paper 2011-01-0626*.

Ntziachristos, L., Giechaskiel, B., Ristimäki, J., and Keskinen, J. (2004). Use of a Corona Charger for the Characterisation of Automotive Exhaust Aerosol. *J. Aerosol Sci.*, 35(8):943–963.

Rostedt, A., Marjamäki, M., and Keskinen, J. (2009a). Modification of the ELPI to Measure Mean Particle Effective Density in Real-Time. *J. Aerosol Sci.,* 40:823–831.

Rostedt, A., Marjamäki, M., Yli-Ojanperä, J., Keskinen, J., Janka, K., Niemelä, V., et al. (2009b). Non-Collecting Electrical Sensor for Particle Concentration Measurement. *AAQR*, 9:470–477.

Tikkanen, J. (2009). Particle Measurement Process and Apparatus. Patent publication no WO 2009/109688.

Whitby, K. T. (1961). Generator for Producing High Concentrations of Small Ions. *Rev. Sci. Instrum.,* 32(12):1351–1355.

Yli-Ojanperä, J., Mäkelä, J. M., Marjamäki, M., Rostedt, A., and Keskinen, J. (2010). Towards Traceable Particle Number Concentration Standard: Single Charged Aerosol Reference (SCAR). *J. Aerosol Sci.*, 41: 719–728.

Yli-Ojanperä, J., Sakurai, H., Iida, K., Mäkelä, J. M., Ehara, K., and Keskinen, J. (2012). Comparison of Three Particle Number Concentration Calibration Standards Through Calibration of a Single CPC in a Wide Particle Size Range. *Aerosol Sci. Technol.*, 46:1163–1173.